

Optical spectral classification of southern ultraluminous infrared galaxies

Jong Chul Lee^{1*}†, Ho Seong Hwang^{2*}, Myung Gyoon Lee^{1‡}, Minjin Kim³, and Sang Chul Kim^{4*}

¹Astronomy Program, Department of Physics and Astronomy, Seoul National University, Seoul 151-742, Korea

²CEA Saclay/Service D’Astrophysique, F-91191 Gif-sur-Yvette, France

³National Radio Astronomy Observatory, 520 Edgemont Road, Charlottesville, VA, USA

⁴Korea Astronomy and Space Science Institute, Daejeon 305-348, Korea

Accepted 2011 January 27. Received 2011 January 26; in original form 2010 December 7

ABSTRACT

We present a study of the optical spectral properties of 115 ultraluminous infrared galaxies (ULIRGs) in the southern sky. Using the optical spectra obtained at CTIO 4 m and provided by the 2dF Galaxy Redshift Survey and the 6dF Galaxy Survey, we measure emission line widths and fluxes for spectral classification. We determine the spectral types of ULIRGs with H α measurement using the standard diagnostic diagrams. For ULIRGs without H α measurement, we determine their spectral types using the plane of flux ratio between [O III] $\lambda 5007$ and H β versus [O III] line width based on our new empirical criterion. This criterion is efficient to distinguish active galactic nuclei (AGNs) from non-AGN galaxies with completeness and reliability of about 90 per cent. The sample of 115 ULIRGs is found to consist of 8 broad-line AGNs, 49 narrow-line AGNs, and 58 non-AGNs. The AGN fraction is on average 50 per cent and increases with infrared luminosity and *IRAS* 25–60 μm colour, consistent with previous studies. The *IRAS* 25–60 μm colour distributions are significantly different between AGN and non-AGN ULIRGs, while their *IRAS* 60–100 μm colour distributions are similar.

Key words: galaxies: active – galaxies: general – galaxies: starburst – infrared: galaxies

1 INTRODUCTION

Ultraluminous infrared galaxies (ULIRGs) with infrared luminosity at 8–1000 μm greater than $10^{12} L_\odot$ (Soifer et al. 1987) are extremely energetic objects in the universe. Although they contribute little to the infrared luminosity density in the local universe due to small numbers, they become cosmologically important at $z > 1$ (e.g., Le Floc’h et al. 2005; Magnelli et al. 2009). Their enormous infrared luminosity comes from dust heated by hot young stars (starburst), a supermassive black hole rapidly accreting matter (active galactic nucleus, AGN), or a mixture of these two (see Sanders & Mirabel 1996 and Lonsdale et al. 2006 for

a review). These starburst and/or AGN activities can be triggered by tidal interactions between galaxies and associated shocks (e.g., Bushouse 1987; Liu & Kennicutt 1995; Barnes 2004). In fact, numerous observational and theoretical studies suggested that ULIRGs are mergers of gas-rich disk galaxies (e.g., Clements et al. 1996; Mihos & Hernquist 1996; Veilleux et al. 2002; Younger et al. 2009; Hwang et al. 2010a), and evolve into quasars (e.g., Sanders et al. 1988; Dasyra et al. 2006; Hopkins et al. 2006; Yuan et al. 2010) or intermediate-mass elliptical galaxies (e.g., Genzel et al. 2001; Tacconi et al. 2002).

To better understand the origin and evolution of ULIRGs, it is essential to find out what their primary energy source is. A standard spectroscopic method to distinguish between starburst and AGN is to use so-called BPT diagrams (Baldwin et al. 1981), which are based on optical emission line ratios sensitive to the photoionization source. This optical diagnostic was revised by Veilleux & Osterbrock (1987) and an alternative scheme was proposed by Kewley et

* Visiting Astronomer, Cerro Tololo Inter-American Observatory, National Optical Astronomy Observatory, which are operated by the Association of Universities for Research in Astronomy, under contract with the National Science Foundation.

† E-mail: jclee@astro.snu.ac.kr

‡ E-mail: mglee@astro.snu.ac.kr

al. (2006). In heavily obscured galaxies like ULIRGs, additional observations at other wavelengths are helpful to characterize their dominant energy source (e.g., X-ray: Franceschini et al. 2003, Teng et al. 2009; infrared: Risaliti et al. 2006, Farrah et al. 2007, Imanishi et al. 2010; radio: Nagar et al. 2003, Sajina et al. 2008). However, it is still difficult to determine the relative contribution of starburst and AGN within individual galaxies.

ULIRGs were discovered in large numbers by the *Infrared Astronomical Satellite* (*IRAS*; Neugebauer et al. 1984) and the number of ULIRGs increased with the advent of wide-field galaxy redshift surveys (Goto 2005; Pasquali et al. 2005; Cao et al. 2006; Hwang et al. 2007, 2010a; Hou et al. 2009). However, previous studies based on optical spectra of the large sample are limited to the Sloan Digital Sky Survey (SDSS; York et al. 2000), which mainly covers the northern hemisphere. The optical spectral properties of ULIRGs in the southern hemisphere remain to be studied.

In this study, we present the analysis of optical spectra for about a hundred southern ULIRGs in the catalogue given by Hwang et al. (2007). The structure of this paper is as follows. The survey data and our observations are described in Section 2. Section 3 explains the procedures to analyse these data and to classify the ULIRGs. In Section 4, the results of our study are discussed, and are compared with those of previous studies. We summarize and conclude in Section 5. Throughout, we adopt $H_0 = 70 \text{ km s}^{-1} \text{ Mpc}^{-1}$ and a flat ΛCDM cosmology with density parameters $\Omega_M = 0.3$ and $\Omega_\Lambda = 0.7$.

2 OBSERVATIONS AND DATA

Hwang et al. (2007) identified 324 ULIRGs by cross-correlating the *IRAS* Faint Source Catalogue Version 2 (Moshir et al. 1992) with the spectroscopic catalogues of galaxies in the Fourth Data Release of SDSS (Adelman-McCarthy et al. 2006.), the Final Data Release of the 2dF Galaxy Redshift Survey (2dFGRS; Colless et al. 2001), and the Second Data Release of the 6dF Galaxy Survey (6dFGS; Jones et al. 2004, 2005). The spectral types of ULIRGs in the SDSS among them were determined in Hou et al. (2009). In this study, we focus on 198 ULIRGs that were not covered by the SDSS but covered by the 2dFGRS and 6dFGS. We used the optical spectra of these ULIRGs available online¹.

The optical spectra of 2dFGRS galaxies were taken with the Two-degree Field (2dF) multi-object spectrograph on the Anglo-Australian Telescope. This spectrograph has 140 μm diameter fibres corresponding to $2''.16$ at the plate centre and $1''.99$ at the edge and covers $3600\text{--}8000 \text{ \AA}$ with a spectral resolution of $\sim 9 \text{ \AA}$. The 6dFGS galaxies were observed with the Six-degree Field (6dF) multi-object spectrograph having $6''.7$ diameter fibres on the United Kingdom Schmidt Telescope. The original grating in the 6dFGS spectrograph spans $4000\text{--}8400 \text{ \AA}$ and gives a resolution of $5\text{--}12 \text{ \AA}$. The improved grating, used after 2002 October, spans $3900\text{--}7500 \text{ \AA}$ with a resolution of $4.9\text{--}6.6 \text{ \AA}$. It is noted

that the 2dFGRS and 6dFGS spectra are not properly flux-calibrated, but the flux ratio of adjacent lines is still useful (to be discussed in Section 4).

In addition, we conducted optical spectroscopy of 15 ULIRGs in the survey sample plus one ULIRG, *IRAS* 09022–3615, in Sanders et al. (2003) at the Cerro Tololo Inter-American Observatory (CTIO). The total number of our ULIRG sample with spectra was increased to 199. The additional ULIRGs were observed on 2008 February 20–21 with the Ritchey-Chretien spectrograph and the Loral 3K CCD at the CTIO 4-m telescope ($0''.5 \text{ pixel}^{-1}$). A slit with a width of $1''.5$ (a slightly larger than the seeing size) was adopted, and was positioned in the east-west direction (P.A. = 90°). We used 316 lines mm^{-1} grating to cover the spectral range $4500\text{--}10500 \text{ \AA}$ with a resolution of 5.6 \AA (~ 2.8 pixels). Three exposures were taken for each object and the integration times ranged from 360 to 3000 seconds depending on its brightness.

Data reduction was performed using the IRAF package. This involved bias subtraction, flat fielding, sky subtraction, wavelength and flux calibration. Galaxy spectra were extracted using an aperture width corresponding to a constant linear scale of 5 kpc at the redshift of each galaxy. A He-Ne-Ar lamp and standard star Hiltner 600 (Massey et al. 1988) taken nightly were used for wavelength and flux calibration, respectively. In Fig. 1, we display 13 spectra with median signal-to-noise ratio (S/N) per pixel for the continuum greater than 3. Typical emission lines ($\text{H}\beta$, $[\text{O III}]\lambda\lambda 4959, 5007$, $\text{H}\alpha + [\text{N II}]\lambda\lambda 6548, 6584$, and $[\text{S II}]\lambda\lambda 6717, 6731$) are clearly seen in most spectra.

Among the sample of 199 ULIRGs considered in this study, we analyse the spectra of 115 ULIRGs with continuum S/N > 3. In the case that there are more than one spectrum for the same object, the spectrum with a higher S/N of $\text{H}\alpha$ flux is chosen for the final classification. If $\text{H}\alpha$ is not available from any spectra, the spectrum with a higher S/N of $\text{H}\beta$ flux has priority.

3 ANALYSIS

3.1 Emission-line measurements

After transforming the spectrum to the rest-frame and subtracting the local continuum defined by a linear fit around emission-lines, we measure the line widths and fluxes via Gaussian profile fit using the MPFIT/IDL package based on the Levenberg-Marquardt method (Markwardt 2009). A single Gaussian is used to obtain the line width of $[\text{O III}]\lambda 5007$. For the line fluxes, we fit the $[\text{O I}]\lambda 6300$ line, $[\text{S II}]\lambda\lambda 6717, 6731$ doublet, $\text{H}\alpha + [\text{N II}]\lambda\lambda 6548, 6584$ and $\text{H}\beta + [\text{O III}]\lambda\lambda 4959, 5007$ line complexes with one Gaussian, two Gaussians, four Gaussians, and six Gaussians, respectively. The widths of the $[\text{N II}]$ doublet are kept the same and the height ratio of $[\text{N II}]\lambda 6548$ to $[\text{N II}]\lambda 6584$ is fixed to 1/3, as required by the energy level structure of the $[\text{N II}]$ ion (Osterbrock & Ferland 2006). The $[\text{O III}]$ doublet is fitted in the same way but each of the $[\text{O III}]$ lines is modelled with two Gaussians because $[\text{O III}]$ line often has a blue, asymmetric wing that is perhaps from outflows of gas with opaque clouds (e.g., Heckman et al. 1981; Greene & Ho 2005). Some AGN host galaxies show both narrow and broad Balmer

¹ For 2dFGRS, <http://www.mso.anu.edu.au/2dFGRS/>
For 6dFGS, <http://www-wfau.roe.ac.uk/6dFGS/>

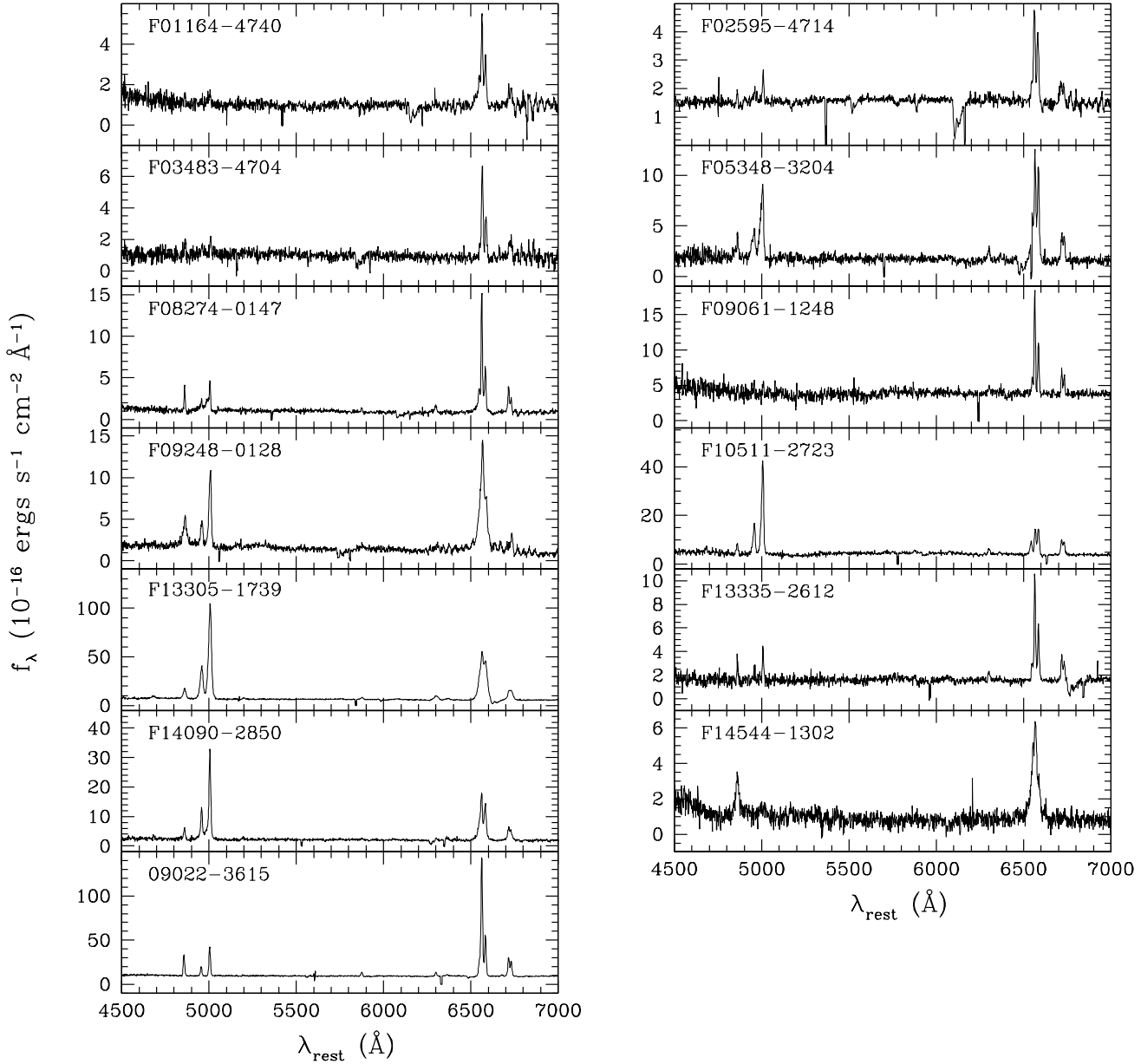


Figure 1. Optical spectra of the ULIRGs observed at CTIO. These spectra are shifted to the rest-frame.

lines (e.g., Osterbrock & Mathews 1986; Hao et al. 2005) and the narrow Balmer lines can have extended bases even in star-forming galaxies, which are probably due to Wolf-Rayet stars (e.g., Osterbrook & Cohen 1982; Brinchmann et al. 2008). To take this into account, we fit each Balmer line with two Gaussians. If the H α +[N II] line complex cannot be decomposed into individual lines, the line fluxes are not kept. Meanwhile, the decomposition of [S II] doublet is not important because we are interested only in the total flux of the lines. Uncertainties in the line measurements, comes from MPFIT routine, are typically 10–30 per cent.

3.2 Corrections

We correct the line fluxes for Galactic extinction using the foreground reddening maps provided by Schlegel et al. (1998) and the extinction law of Cardelli et al. (1989).

Balmer emission lines can be strongly affected by stellar absorption features. We remove the stellar absorption effects following the method discussed in Hopkins et al. (2003): $S = F(EW + EW_c)/EW$, where S is the stellar absorption-corrected line flux, F is the measured line flux after foreground reddening correction, EW is the equivalent width of

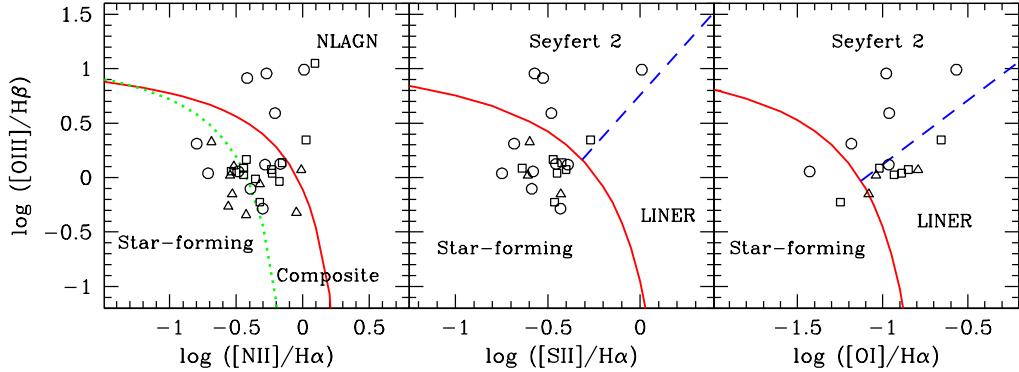


Figure 2. The diagnostic diagrams for ULIRGs in the Sample A. CTIO, 2dFGRS, and 6dFGS samples are represented by circle, square, and triangle, respectively. The solid, dotted, and dashed lines indicate the extreme starburst (Kewley et al. 2001), pure star formation (Kauffmann et al. 2003), and Seyfert-LINER (Kewley et al. 2006) lines, respectively. NLAGN represents narrow-line AGN.

the line, and EW_c is a correction factor. We adopted EW_c values (2.6 and 3.2 Å for H α and H β , respectively) of Sc type galaxies (Miller & Owen 2002).

If both H α and H β are measured, we can correct the line fluxes for internal extinction using the Balmer decrement and the extinction curve with an assumption of an intrinsic H α /H β line ratio of 2.85 for star-forming galaxies and 3.1 for AGN galaxies (Osterbrock & Ferland 2006). We do not apply this correction when the observed ratio is smaller than the theoretical value.

An observed line width is the convolution of intrinsic line width and instrumental response. Since the instrumental resolution of each survey is significantly different, the observed line width should be corrected for a fair comparison. To correct the full width at half maximum (FWHM) of [O III] $\lambda\lambda 5007$ line using the quadrature method, we adopt 250 km s $^{-1}$ as a finite resolution of CTIO spectra. Then we determine that the resolutions are roughly 450, 600, and 400 km s $^{-1}$ for the 2dFGRS, original 6dFGS, and improved 6dFGS grating, respectively, by considering that the [O III] lines from different spectra have the same intrinsic width. Note that corrected line widths below 100 km s $^{-1}$ should be treated with caution due to their large uncertainties (> 200 km s $^{-1}$).

3.3 Spectral classification

We use the emission lines with flux uncertainty $< 60\%$ for spectral classification. The qualities of line fluxes with uncertainty $< 20\%$, 20–40%, and 40–60% are referred to hereafter as high, moderate, and low, respectively (see Tables 2 and 3).

In the sample of 115 ULIRGs, 8 ULIRGs have broad Balmer lines, FWHM of broad component of Balmer lines > 2000 km s $^{-1}$ and height of the broad component > 3 times the local rms of the continuum-subtracted spectra. These are considered to be broad-line AGN galaxies².

There are 32 narrow emission-line ULIRGs for which

² In Table 1, we use the term “Seyfert 1 galaxies” to indicate broad-line AGNs, which is commonly used in previous studies.

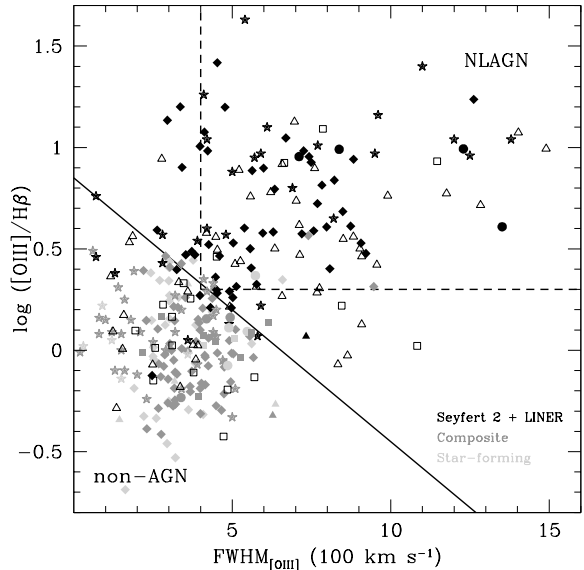


Figure 3. $\log([O\text{III}]/H\beta)$ vs. $\text{FWHM}_{[O\text{III}]}$ diagram for the Sample B ULIRGs, which are denoted by open symbols. The ULIRGs already classified in the diagnostic diagrams are overplotted by filled symbols (black: Seyfert 2 plus LINER; dark-grey: composite; light-grey: star-forming). Circles, squares, and triangles represent CTIO, 2dFGRS, and 6dFGS ULIRGs, respectively. Stars and diamonds represent ULIRGs from the 1 Jy sample (Veilleux et al. 1999; Yuan et al. 2010) and the SDSS sample (Hou et al. 2009), respectively. The dashed and solid lines show the criteria of Zakamska et al. (2003) and our new boundary separating narrow-line AGNs (NLAGNs) and non-AGNs. In this diagram, [O III]/H β line ratios are corrected only for Galactic extinction and stellar absorption.

more than two line ratios ([O III] $\lambda 5007$ /H β and at least one of [N II] $\lambda 6584$ /H α , [S II] $\lambda\lambda 6717, 6731$ /H α , and [O I] $\lambda 6300$ /H α) were measured (hereafter Sample A). In Fig. 2, we show the diagnostic diagrams for these ULIRGs and divide them into star-forming, (starburst-AGN) composite, and narrow-line AGN galaxies based on their loci in the

Table 1. Basic information and spectral types of 115 southern ULIRGs.

<i>IRAS</i> name	RA (J2000)	Dec (J2000)	z	f_{25}	f_{60}	f_{100}	$\log \frac{L_{\text{IR}}}{L_{\odot}}$	sample	class	sub.	known
F00050–3259	00 07 34.6	−32 43 03	0.285	<0.144	0.222	<0.758	12.12	2dFGRS	X		
F00091–3905	00 11 42.3	−38 49 15	0.253	<0.125	0.316	<0.756	12.14	6dFGS	N		
F00184–3331	00 20 57.7	−33 14 28	0.238	<0.120	0.334	0.613	12.10	2dFGRS	X		
F00318–3137	00 34 16.0	−31 21 04	0.284	<0.167	0.257	0.563	12.18	6dFGS	X		
F00335–2732	00 35 59.2	−27 15 42	0.068	0.632	4.294	3.207	12.01	2dFGRS	X	Co	Co(5)
F00456–2904	00 48 03.5	−28 48 38	0.110	0.141	2.598	3.377	12.23	2dFGRS	X	Co	Co(5)
F00482–2721	00 50 40.0	−27 04 42	0.129	<0.182	1.134	1.839	12.03	2dFGRS	X	Co	Co(5)
F00569–3108	00 59 22.3	−30 52 27	0.344	<0.055	0.239	<0.463	12.34	6dFGS	N		
F01004–2237	01 02 51.2	−22 21 50	0.117	0.660	2.287	1.790	12.24	6dFGS	N		Co(5) ^a
F01009–3241	01 03 19.8	−32 25 37	0.256	<0.123	0.291	<0.750	12.12	2dFGRS	N		
F01160–2551	01 18 24.2	−25 36 19	0.237	<0.138	0.452	1.153	12.23	2dFGRS	X		
F01164–4740	01 18 36.5	−47 25 04	0.235	<0.219	0.487	0.674	12.25	CTIO	X	SF	
F01212–5025	01 23 20.1	−50 09 29	0.201	<0.077	0.415	0.717	12.02	6dFGS	N		
F01234–0447	01 25 56.0	−04 31 57	0.156	<0.162	0.711	1.108	12.01	6dFGS	X		
F01358–3300	01 38 05.3	−32 45 29	0.197	<0.138	0.835	1.079	12.31	2dFGRS	X		SF(1)
F01379–3203	01 40 15.3	−31 48 18	0.202	<0.146	0.686	0.929	12.25	6dFGS	N		
F01497–2906	01 52 04.0	−28 51 18	0.183	<0.052	0.588	1.278	12.08	2dFGRS	X	Co	
F01569–2939	01 59 13.1	−29 24 37	0.140	0.143	1.734	1.514	12.29	2dFGRS	N		Co(5) ^a
F02038–0816	02 06 18.7	−08 02 32	0.220	<0.326	0.351	0.525	12.04	6dFGS	N		
F02068–2000	02 09 09.0	−19 46 30	0.253	<0.190	0.278	<0.647	12.09	6dFGS	N		
F02130–1948	02 15 23.5	−19 34 18	0.191	<0.196	0.553	0.565	12.10	6dFGS	N		
F02356–4628	02 37 29.3	−46 15 48	0.206	<0.090	1.034	1.738	12.45	2dFGRS	X		
F02361–3233	02 38 15.2	−32 20 34	0.198	<0.073	0.741	1.821	12.26	2dFGRS	X	SF	
F02364–4751	02 38 13.6	−47 38 06	0.097	0.175	2.794	4.953	12.15	6dFGS	N		
F02384–1744	02 40 46.4	−17 31 52	0.308	<0.072	0.269	<1.344	12.28	6dFGS	X		
F02437–1145	02 46 07.8	−11 32 42	0.270	0.148	0.208	<0.710	12.03	6dFGS	B	S1	
F02595–4714	03 01 18.4	−47 02 17	0.245	<0.063	0.268	0.484	12.04	CTIO	X	Co	
F03000–2719	03 02 10.6	−27 07 29	0.221	<0.113	0.918	2.039	12.47	2dFGRS	N		
F03130–3119	03 15 04.6	−31 08 02	0.258	<0.103	0.252	0.438	12.06	2dFGRS	X		
F03259–3105	03 27 59.3	−30 54 50	0.261	<0.065	0.249	0.559	12.07	2dFGRS	X		
F03483–4704	03 49 54.4	−46 55 10	0.301	<0.098	0.156	<0.542	12.02	CTIO	X	SF	
F03485–1827	03 50 45.7	−18 18 27	0.174	0.164	0.580	<0.822	12.03	6dFGS	N		
F03569–2535	03 59 00.9	−25 26 44	0.220	0.071	0.613	0.598	12.28	6dFGS	X		
F04056–5722	04 06 41.9	−57 14 38	0.267	0.079	0.259	0.453	12.11	6dFGS	X		
F04279–3035	04 29 55.7	−30 28 54	0.232	<0.114	0.311	<0.839	12.04	6dFGS	X		
F04489–1026	04 51 19.5	−10 21 22	0.231	<0.090	0.357	<1.767	12.10	6dFGS	N		
F04505–2958	04 52 30.7	−29 53 34	0.285	0.189	0.650	0.765	12.58	6dFGS	B	S1	S1(4)
F05020–2941	05 04 00.8	−29 36 57	0.154	0.102	1.932	2.059	12.43	6dFGS	X		Co(5)
F05156–3024	05 17 31.9	−30 21 14	0.171	0.103	1.162	1.402	12.31	6dFGS	N		S2(5)
F05348–3204	05 36 44.9	−32 02 20	0.174	0.224	0.623	0.712	12.06	CTIO	N	S2	
F06158–4017	06 17 29.8	−40 18 57	0.221	0.083	0.311	<0.707	12.00	6dFGS	N		
F08274–0147	08 30 00.6	−01 57 05	0.250	0.149	0.594	0.622	12.40	CTIO	X	SF	
F08411–2501	08 43 18.8	−25 11 58	0.134	0.262	1.655	1.572	12.23	6dFGS	N		
F09061–1248	09 08 35.1	−13 01 01	0.073	0.191	3.634	5.316	12.01	CTIO	X	Co	SF(2)
F09090–1349	09 11 27.9	−14 01 40	0.171	<0.091	0.845	1.553	12.17	6dFGS	X		
F09248–0128	09 27 23.9	−01 41 19	0.324	<0.102	0.221	<0.667	12.25	CTIO	B	S1	
F09521–0400	09 54 37.2	−04 15 12	0.237	<0.108	0.387	0.600	12.16	2dFGRS	N		
F10077+0034	10 10 16.6	00 19 31	0.182	<0.127	0.513	0.834	12.02	2dFGRS	X	SF	
F10298–2300	10 32 11.7	−23 15 41	0.285	<0.153	0.377	<1.583	12.35	6dFGS	N		
F10479–2808	10 50 18.9	−28 24 01	0.191	0.327	1.002	1.151	12.36	6dFGS	B	S1	
F10511–2723	10 53 33.3	−27 39 05	0.159	0.319	0.896	<1.351	12.13	CTIO	N	S2	
F10533–3534	10 55 40.2	−35 50 06	0.190	<0.096	0.556	<1.153	12.09	6dFGS	X	Co	
F10549–3702	10 57 18.5	−37 18 25	0.216	<0.077	0.348	<1.265	12.02	6dFGS	N		
F11053–2413	11 07 47.0	−24 29 25	0.225	<0.092	0.314	<2.103	12.02	6dFGS	N		
F11093–3353	11 11 45.4	−34 09 35	0.231	0.102	0.318	0.894	12.05	6dFGS	X	SF	
F11095–0238	11 12 02.5	−02 54 18	0.106	0.418	3.249	2.531	12.30	2dFGRS	X	Co	Co(5)
F11204–2154	11 22 58.0	−22 11 02	0.248	<0.114	0.264	<1.263	12.04	6dFGS	X		
F11300–0522	11 32 41.4	−05 39 41	0.230	<0.164	0.668	1.610	12.37	2dFGRS	X		
F11451–2128	11 47 39.0	−21 45 06	0.219	<0.182	0.375	<0.859	12.07	6dFGS	B	S1	
F12131–2809	12 15 42.4	−28 26 19	0.360	<0.102	0.325	<1.811	12.52	6dFGS	N		
F12432–3138	12 45 57.2	−31 54 42	0.423	<0.154	0.256	<0.718	12.61	6dFGS	N		
F12452–2032	12 47 53.6	−20 48 24	0.209	<0.203	0.383	<0.988	12.03	6dFGS	X		
F13269–2251	13 29 40.8	−23 07 10	0.290	<0.114	0.382	<1.410	12.37	6dFGS	X		

Table 1. – Continued.

<i>IRAS</i> name	RA (J2000)	Dec (J2000)	z	f_{25}	f_{60}	f_{100}	$\log \frac{L_{\text{IR}}}{L_{\odot}}$	sample	class	sub.	known
F13270–0331	13 29 40.7	−03 46 59	0.221	<0.306	0.954	0.797	12.48	2dFGRS	N		
F13305–1739	13 33 15.2	−17 55 00	0.148	0.392	1.164	1.044	12.17	CTIO	N	S2	S2(5)
F13306–1644	13 33 21.5	−17 00 22	0.231	<0.208	0.298	<0.752	12.02	6dFGS	X		
F13335–2612	13 36 22.1	−26 27 30	0.125	<0.139	1.402	2.101	12.09	CTIO	X	Co	Co(5)
F13379–0256	13 40 33.4	−03 11 42	0.218	<0.235	0.728	1.032	12.35	2dFGRS	X		
F13531–3422	13 56 06.6	−34 37 02	0.220	0.135	0.380	<0.777	12.08	6dFGS	N		
F14021–3139	14 05 02.1	−31 54 17	0.202	<0.178	0.568	<1.124	12.17	6dFGS	N		
F14090–2850	14 11 59.2	−29 05 01	0.212	0.197	0.507	<0.807	12.17	CTIO	N	S2	
F14121–0126	14 14 45.7	−01 40 53	0.150	<0.239	1.394	2.073	12.26	2dFGRS	X	Co	S2(5) ^a
F14207–2002	14 23 31.5	−20 15 47	0.173	<0.208	0.850	1.082	12.18	6dFGS	N		S2(1)
F14248–3644	14 27 51.7	−36 58 03	0.208	<0.122	0.450	<1.499	12.10	6dFGS	X		
F14254–2655	14 28 19.9	−27 08 49	0.253	<0.206	0.534	0.809	12.37	6dFGS	N		S2(1)
F14348–1447	14 37 37.2	−15 00 20	0.082	0.495	6.870	7.068	12.39	6dFGS	X	SF	Co(5) ^a
F14544–1302	14 57 09.5	−13 14 55	0.254	<0.265	0.309	<0.761	12.13	CTIO	B	S1	
F15130–1958	15 15 55.5	−20 09 17	0.108	0.388	1.916	2.299	12.09	6dFGS	N		S2(3)
F16090–0139	16 11 40.9	−01 47 06	0.134	0.264	3.609	4.874	12.57	6dFGS	X	Co	Co(3) ^b
F16159–0402	16 18 36.3	−04 09 42	0.211	0.299	0.979	<1.768	12.45	6dFGS	N		
F19466–3649	19 49 55.5	−36 42 06	0.093	0.316	2.425	3.378	12.05	6dFGS	X	SF	
F19548–6237	19 59 18.9	−62 29 18	0.351	<0.081	0.365	<0.823	12.55	6dFGS	X		
F20023–5253	20 06 08.1	−52 44 48	0.238	<0.089	0.312	<1.454	12.07	6dFGS	X		
F20066–1630	20 09 27.7	−16 22 06	0.163	<0.146	0.639	<1.285	12.00	6dFGS	X		
F20181–2244	20 21 03.9	−22 35 22	0.184	<0.199	0.568	0.885	12.07	6dFGS	N		
F20248–3204	20 27 59.1	−31 54 54	0.203	<0.119	0.440	<2.673	12.06	6dFGS	X		
F20270–4237	20 30 24.9	−42 27 24	0.242	<0.102	0.287	<0.646	12.05	6dFGS	N		
F20273–6558	20 31 50.8	−65 48 22	0.349	0.155	0.430	<1.151	12.61	6dFGS	N		
F20542–1832	20 57 03.6	−18 20 43	0.298	<0.126	0.322	0.934	12.33	6dFGS	N		
F20551–4250	20 58 27.3	−42 38 57	0.042	1.906	12.780	9.948	12.06	6dFGS	X	SF	Co(5) ^a
F21016–1900	21 04 29.8	−18 48 17	0.230	<0.230	0.305	1.025	12.03	6dFGS	N		
F21356–1015	21 38 20.2	−10 01 57	0.206	0.159	0.460	0.550	12.09	6dFGS	N		
F21367–2405	21 39 36.6	−23 51 51	0.234	<0.102	0.383	0.565	12.15	6dFGS	X	SF	
F21435–3648	21 46 31.9	−36 34 54	0.160	<0.149	0.665	0.999	12.01	6dFGS	N		
F21488–2819	21 51 41.4	−28 05 14	0.234	<0.135	0.301	<0.677	12.04	2dFGRS	X		
F21542–4050	21 57 21.3	−40 36 03	0.301	<0.093	0.253	<0.531	12.23	6dFGS	B	S1	
F21555–4235	21 58 37.5	−42 21 33	0.181	<0.132	0.833	0.987	12.22	6dFGS	X		
F22058–3501	22 08 48.8	−34 46 38	0.173	<0.162	0.561	1.375	12.01	2dFGRS	N		
F22206–2715	22 23 29.4	−26 59 59	0.131	<0.159	1.754	2.333	12.23	2dFGRS	X	Co	Co(5)
F22301–2822	22 32 56.7	−28 07 17	0.244	<0.123	0.312	<0.925	12.10	2dFGRS	N		
F22423–4707	22 45 20.2	−46 52 03	0.200	0.150	0.451	0.693	12.05	6dFGS	B	S1	
F22521–3929	22 54 56.5	−39 13 14	0.261	0.135	0.283	<0.545	12.13	6dFGS	N		
F22546–2637	22 57 23.8	−26 21 23	0.163	<0.166	0.752	1.362	12.08	2dFGRS	X		SF(1)
F22560–3501	22 58 46.7	−34 45 44	0.171	0.141	0.593	0.795	12.02	2dFGRS	X	Co	
F23046–3454	23 07 21.3	−34 38 41	0.208	<0.093	0.937	1.313	12.41	2dFGRS	X		
F23128–5919	23 15 46.5	−59 03 14	0.044	1.590	10.800	10.990	12.03	6dFGS	X	SF	
F23142–0611	23 16 49.3	−05 55 13	0.346	<0.158	0.263	<0.405	12.39	6dFGS	N		
F23185–0328	23 21 05.9	−03 12 03	0.246	<0.228	0.308	<0.385	12.10	6dFGS	N		
F23206–1222	23 23 14.4	−12 06 29	0.249	<0.255	0.246	<0.689	12.01	2dFGRS	N		
F23242–0357	23 26 49.1	−03 41 18	0.189	<0.275	0.454	0.566	12.00	6dFGS	X		
F23253–5415	23 28 06.0	−53 58 26	0.129	0.214	2.296	3.493	12.34	6dFGS	N	LI	
F23516–2420	23 54 13.0	−24 04 05	0.154	<0.283	0.834	1.240	12.06	6dFGS	X		
F23529–2119	23 55 33.8	−21 02 49	0.428	<0.156	0.327	0.627	12.73	6dFGS	N		
F23559–3009	23 58 31.0	−29 52 18	0.342	<0.152	0.237	<0.463	12.33	2dFGRS	X		
09022–3615	09 04 12.8	−36 27 02	0.059	1.154	11.470	11.080	12.26	CTIO	X	SF	

Column descriptions: (1) Object name in the *IRAS* catalogue. (2-3) Right ascension and declination in units of $^h m s$ and $^{\circ} ' ''$, respectively. (4) Redshift. (5-7) The *IRAS* flux density at 25, 60, and 100 μm [Jy]. (8) Infrared luminosity. (1-8) Basic information taken from Hwang et al. (2007) except 09022–3615, for which information was taken from Sanders et al. (2003). (9) Adopted spectrum. (10) Spectral class in this study (B=broad-line AGN, N=narrow-line AGN, X=non-AGN). (11) Subclass in this study (S1=Seyfert 1, S2=Seyfert 2, LI=LINER, Co=composite, SF=star-forming galaxy). (12) Subclass from previous studies. Numbers in parentheses are references (1=Allen et al. 1991, 2=Duc et al. 1997, 3=Kim et al. 1998, 4=Low et al. 1988, 5=Yuan et al. 2010).

^a The spectral types of these objects are different between this study and previous studies.

^b This object was classified as a LINER by Kim et al. (1998) using the Veilleux & Osterbrock (1987) scheme.

Table 2. Line information of the Sample A ULIRGs.

<i>IRAS</i> name	quality	$f_{H\alpha}$	$EW_{H\alpha}$	$\frac{H\alpha}{H\beta}$	$FWHM_{[O\text{ III}]}$	$\log \frac{[O\text{ III}]}{H\beta}$	$\log \frac{[N\text{ II}]}{H\alpha}$	$\log \frac{[S\text{ II}]}{H\alpha}$	$\log \frac{[O\text{ I}]}{H\alpha}$
F00335–2732	3333333	...	50	5.81	559±23	0.06±0.10	-0.44±0.06	-0.66±0.10	-0.99±0.10
F00456–2904	3333333	...	78	4.75	394±16	-0.25±0.03	-0.33±0.02	-0.48±0.04	-1.23±0.09
F00482–2721	2323320	...	40	5.44	445±76	0.01±0.19	-0.23±0.06	-0.49±0.30	-0.86±0.22
F01164–4740	1103322	8.5	86	10.88	489±168	0.04±0.45	-0.71±0.16	-0.75±0.25	...
F01497–2906	3203300	...	47	4.09	526±74	-0.06±0.23	-0.18±0.12
F01569–2939	3333333	...	97	5.58	636±8	0.32±0.03	0.02±0.02	-0.28±0.06	-0.63±0.03
F02361–3233	3303300	...	72	5.14	507±21	0.03±0.10	-0.54±0.10
F02595–4714	2303321	3.9	25	5.69	493±45	0.12±0.18	-0.17±0.06	-0.46±0.29	...
F03483–4704	1203311	6.5	72	4.78	485±64	-0.10±0.35	-0.39±0.10	-0.59±0.35	...
F05348–3204	1323322	16.5	99	4.24	1351±38	0.59±0.22	-0.21±0.06	-0.48±0.21	-0.96±0.25
F08274–0147	3323333	20.4	236	8.18	573±88	0.31±0.08	-0.80±0.07	-0.68±0.11	-1.18±0.20
F09061–1248	1103332	13.4	36	7.72	338±145	-0.29±0.38	-0.30±0.10	-0.43±0.23	...
F10077+0034	2222300	...	66	4.55	410±56	0.03±0.25	-0.44±0.21	...	-0.93±0.30
F10511–2723	2323332	12.5	25	2.26	837±10	0.99±0.13	0.01±0.07	0.01±0.17	-0.57±0.19
F10533–3534	2103300	...	201	1.71	...	-0.06±0.46	-0.32±0.17
F11093–3353	2102200	...	36	1.31	636±157	-0.27±0.40	-0.56±0.31
F11095–0238	3232322	...	54	5.39	409±40	0.07±0.28	-0.24±0.26	-0.40±0.29	-0.85±0.30
F13305–1739	3333330	128.5	228	6.15	1229±9	0.96±0.08	-0.27±0.05	-0.57±0.04	-0.98±0.06
F13335–2612	2323321	9.0	58	5.66	418±52	0.12±0.20	-0.28±0.20	-0.39±0.38	-0.96±0.37
F14090–2850	3303332	33.3	161	6.76	710±12	0.91±0.08	-0.42±0.09	-0.53±0.18	...
F14121–0126	2103332	...	68	10.40	615±51	0.07±0.41	-0.16±0.13	-0.46±0.18	...
F14348–1447	3333333	...	99	4.68	...	-0.01±0.11	-0.55±0.09	-0.62±0.16	-1.02±0.20
F16090–0139	2103300	...	27	2.13	627±176	-0.32±0.40	-0.05±0.17
F19466–3649	2103300	...	15	3.78	143±120	-0.37±0.43	-0.42±0.10
F20551–4250	3333333	...	60	3.92	318±13	-0.17±0.03	-0.53±0.04	-0.44±0.05	-1.07±0.06
F21367–2405	3303300	...	91	1.23	...	0.10±0.11	-0.52±0.13
F22058–3501	1302300	...	19	13.34	407±20	0.97±0.17	0.09±0.33
F22206–2715	2203300	...	43	6.97	217±76	-0.06±0.19	-0.36±0.05
F22560–3501	2202322	...	51	3.78	274±66	0.15±0.32	-0.42±0.29	-0.48±0.28	...
F23128–5919	3302222	...	52	2.57	360±19	0.33±0.17	-0.69±0.41	-0.60±0.31	...
F23253–5415	3223300	...	40	2.04	733±99	0.07±0.30	-0.01±0.06	...	-0.79±0.23
09022–3615	3333333	154.7	164	5.67	547±11	0.06±0.04	-0.48±0.16	-0.58±0.16	-1.43±0.19

Column descriptions: (1) Object name in the *IRAS* catalogue. (2) Line flux qualities at $H\beta$, $[O\text{ III}]\lambda 5007$, $[O\text{ I}]\lambda 6300$, $H\alpha$, $[N\text{ II}]\lambda 6584$, $[S\text{ II}]\lambda 6717$, and $[S\text{ II}]\lambda 6731$ (0=unmeasurable, 1=low, 2=moderate, 3=high). (3) Absolute flux of $H\alpha$ [$10^{-15}\text{ ergs s}^{-1}\text{ cm}^{-2}$]. The values from uncalibrated spectra are not presented. (4) Equivalent width of $H\alpha$ [Å]. (5) Observed $H\alpha/H\beta$ line ratio. (6) $[O\text{ III}]$ line width after instrumental resolution correction and its uncertainty [km s^{-1}]. Line widths below 100 km s^{-1} are not shown. (7-10) Logarithms of the line ratios and their uncertainties. The ratios are corrected for Galactic extinction and stellar absorption. The internal extinction correction is applied, if available.

diagrams. Star-forming galaxies lie below the pure star formation line (Kauffmann et al. 2003) in the $[N\text{ II}]/H\alpha$ diagram and lie below the extreme starburst line (Kewley et al. 2001) in other diagrams. Composite galaxies lie between the extreme starburst line and the pure star formation line in the $[N\text{ II}]/H\alpha$ diagram. Narrow-line AGNs lie above the extreme starburst line in all three diagrams. Whenever possible, narrow-line AGNs are subdivided into Seyfert 2 and low ionization narrow emission-line region (LINER) galaxies. Seyfert 2 galaxies lie above the Seyfert-LINER classification lines (Kewley et al. 2006) in the $[S\text{ II}]/H\alpha$ and $[O\text{ I}]/H\alpha$ diagrams, whereas LINERs lie below the lines. For ambiguous galaxies that are classified as one type in two diagrams but another type in the remaining diagram, we adopt the types that are given in the first two diagrams.

There are 75 narrow emission-line ULIRGs without measurable $H\alpha$ line mainly because $H\alpha$ falls outside the spectral coverage (hereafter Sample B). These galaxies could not be classified in the diagnostic diagrams so that we attempt to classify them in flux ratio between $[O\text{ III}]$ and

$H\beta$ lines versus $[O\text{ III}]$ line width diagram as demonstrated in Fig. 3. Zakamska et al. (2003) used the criteria of $\log([O\text{ III}]/H\beta) > 0.3$ and $FWHM_{[O\text{ III}]} > 400\text{ km s}^{-1}$ to select narrow-line AGN galaxies (dashed line). Using our Sample A and two large, homogeneous samples in the literature (the *IRAS* 1 Jy ULIRGs: Kim & Sanders 1998; Veilleux et al. 1999; Yuan et al. 2010; the SDSS ULIRGs: Hou et al. 2009), we determine a new boundary to separate narrow-line AGN galaxies from the others (solid line) with high completeness and reliability as far as possible: $\log([O\text{ III}]/H\beta) > -0.13 (FWHM_{[O\text{ III}]} / 100\text{ km s}^{-1}) + 0.85$. If we regard AGNs classified in the diagnostic diagrams as genuine AGNs, the application of our new boundary provides 89% completeness (among the total 88 AGNs, 78 AGNs are found inside this boundary) and 89% reliability (among 88 objects in the boundary, 78 objects are AGNs), while 68% (60/88) completeness and 90% (60/67) reliability using the criteria of Zakamska et al. The galaxies outside the boundary are mostly star-forming or composite galaxies,

Table 3. Line information of the Sample B ULIRGs.

<i>IRAS</i> name	quality	FWHM _[O III]	$\log \frac{[O\text{ III}]}{H\beta}$	<i>IRAS</i> name	quality	FWHM _[O III]	$\log \frac{[O\text{ III}]}{H\beta}$
F00050–3259	33	378±41	-0.11±0.14	F12432–3138	12	701±66	0.74±0.39
F00091–3905	12	621±102	0.78±0.40	F12452–2032	33	185±53	0.56±0.13
F00184–3331	11	472±141	-0.43±0.38	F13269–2251	11	384±93	-0.05±0.51
F00318–3137	22	...	0.26±0.30	F13270–0331	33	1146±8	0.93±0.14
F00569–3108	12	...	0.84±0.52	F13306–1644	12	175±48	0.53±0.34
F01004–2237	32	850±28	0.55±0.16	F13379–0256	23	310±58	0.02±0.16
F01009–3241	33	786±13	1.09±0.07	F13531–3422	23	760±23	0.90±0.19
F01160–2551	33	250±54	-0.15±0.09	F14021–3139	12	575±87	0.31±0.37
F01212–5025	22	908±134	0.13±0.39	F14207–2002	12	448±91	0.56±0.53
F01234–0447	22	...	-0.17±0.20	F14248–3644	12	331±90	0.34±0.41
F01358–3300	22	368±18	0.25±0.09	F14254–2655	11	711±61	0.62±0.45
F01379–3203	23	1176±27	0.77±0.19	F15130–1958	12	1283±75	0.72±0.47
F02038–0816	13	277±28	0.94±0.38	F16159–0402	11	833±134	-0.07±0.43
F02068–2000	22	...	0.52±0.25	F19548–6237	11	335±119	-0.18±0.51
F02130–1948	12	657±83	0.27±0.29	F20023–5253	12	376±135	0.03±0.35
F02356–4628	33	569±45	-0.13±0.15	F20066–1630	32	134±102	-0.28±0.30
F02364–4751	33	508±40	0.43±0.10	F20181–2244	33	882±12	0.56±0.12
F02384–1744	12	248±66	-0.07±0.43	F20248–3204	12	359±120	0.29±0.54
F03000–2719	23	664±17	0.92±0.02	F20270–4237	12	696±78	1.13±0.37
F03130–3119	11	281±83	0.22±0.47	F20273–6558	13	1402±70	1.07±0.30
F03259–3105	31	256±36	0.01±0.32	F20542–1832	23	418±24	0.58±0.22
F03485–1827	33	657±11	0.92±0.12	F21016–1900	12	863±165	-0.03±0.31
F03569–2535	23	157±37	0.17±0.19	F21356–1015	23	902±12	0.50±0.20
F04056–5722	32	...	0.27±0.18	F21435–3648	13	557±25	0.76±0.18
F04279–3035	23	116±37	0.36±0.20	F21488–2819	33	346±13	0.33±0.09
F04489–1026	13	525±53	0.44±0.19	F21555–4235	33	123±32	0.09±0.14
F05020–2941	33	154±46	0.01±0.15	F22301–2822	32	1083±113	0.02±0.19
F05156–3024	23	990±28	0.76±0.17	F22521–3929	13	775±79	0.31±0.40
F06158–4017	22	767±52	0.28±0.28	F22546–2637	23	194±37	0.10±0.16
F08411–2501	31	908±149	0.46±0.41	F23046–3454	33	309±23	0.17±0.10
F09090–1349	12	...	-0.07±0.52	F23142–0611	22	452±51	0.50±0.38
F09521–0400	12	845±94	0.22±0.40	F23185–0328	33	956±32	0.42±0.15
F10298–2300	23	1490±71	0.99±0.24	F23206–1222	33	451±5	0.46±0.15
F10549–3702	12	491±112	0.22±0.28	F23242–0357	22	...	0.20±0.38
F11053–2413	13	521±55	0.89±0.44	F23516–2420	21	...	-0.39±0.43
F11204–2154	22	391±87	0.02±0.36	F23529–2119	12	634±106	0.50±0.51
F11300–0522	32	...	-0.45±0.26	F23559–3009	11	485±71	-0.19±0.54
F12131–2809	23	713±40	0.47±0.17				

Column descriptions: (1, 5) Object name in the *IRAS* catalogue. (2, 6) Line flux qualities at H β and [O III] $\lambda 5007$ (0=unmeasurable, 1=low, 2=moderate, 3=high). (3, 7) [O III] line width after instrumental resolution correction and its uncertainty [km s $^{-1}$]. Line widths below 100 km s $^{-1}$ are not presented. (4, 8) Logarithm of [O III]/H β line ratio and its uncertainty. The ratio is corrected only for Galactic extinction and stellar absorption.

but they are not separable from each other in this diagram. They are referred to as non-AGN galaxies.

Our 115 southern ULIRGs contain 8 broad-line AGNs, 49 narrow-line AGNs including four Seyfert 2 and one LINER galaxies, and 58 non-AGNs including thirteen composite and twelve star-forming galaxies. The spectral classification results (and their basic information) are presented in Table 1. Detailed line information of Samples A and B is listed in Tables 2 and 3, respectively.

4 DISCUSSION

4.1 Reliability of our spectral classification

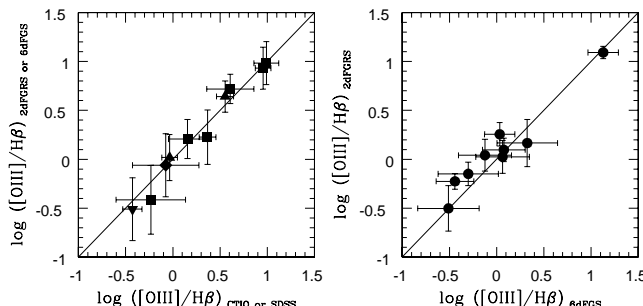
The small aperture spectroscopy could not always contain enough light of an extended source to determine its spec-

tral type. For reliable classification, it is suggested to use an aperture covering more than $\sim 20\%$ of the galaxy light. The minimum aperture covering fraction of 20% corresponds to 2.1 kpc (see fig. 6 in Kewley et al. 2005). All spectra of ULIRGs in this study satisfy this condition. Therefore, aperture-related effects on our classification are expected to be negligible.

In the 2dFGRS and 6dFGS spectra, the flux for individual line can be unreliable because these spectra are not properly flux-calibrated. Nevertheless, the flux ratio between lines with similar wavelengths is still useful (e.g., Mouhcine et al. 2005; Owers et al. 2007). To ensure this, in Fig. 4, we compare [O III]/H β line ratios derived from both calibrated (i.e., CTIO or SDSS) and uncalibrated (i.e., 2dFGRS or 6dFGS) spectra. It shows that two measurements agree

Table 4. AGN fraction as a function of infrared properties

sample	$\log(L_{\text{IR}}/L_{\odot})$			
	all	[12.0, 12.15)	[12.15, 12.4)	[12.4, 13.0)
This study	50% of 115	48% of 61	50% of 40	57% of 14
Kim & Sanders (1998)	45% of 108	38% of 40	39% of 49	79% of 19
Hou et al. (2009)	55% of 209	43% of 90	51% of 81	89% of 36
sample	$\log(f_{25}/f_{60})$			
	all	[-1.4, -0.9)	[-0.9, -0.5)	[-0.5, -0.1)
This study	59% of 37	40% of 10	47% of 15	92% of 12
Kim & Sanders (1998)	56% of 59	29% of 28	76% of 25	100% of 6
Hou et al. (2009)	53% of 45	33% of 18	38% of 13	93% of 14
sample	$\log(f_{60}/f_{100})$			
	all	[-0.7, -0.3)	[-0.3, -0.1)	[-0.1, 0.3)
This study	40% of 70	36% of 11	33% of 36	52% of 23
Kim & Sanders (1998)	45% of 108		33% of 51	56% of 57
Hou et al. (2009)	43% of 106	58% of 19	39% of 61	46% of 24

**Figure 4.** Comparison of [O III]/H β line ratio between two spectra. In the left panel, the measurements from CTIO-6dFGS, CTIO-2dFGRS, SDSS-6dFGS, and SDSS-2dFGRS are denoted by squares, diamonds, triangles, and inverse triangles, respectively. In the right panel, the measurements from 6dFGS-2dFGRS are denoted by circles. Only objects with S/Ns of both spectra > 3 are presented. The one-to-one relation (solid line) is overplotted.

well within the errors. The measurements between the 2dFGRS and 6dFGS spectra also agree well.

Among the 115 ULIRGs, there are 22 objects whose spectral types have been previously determined in the literature. The spectral types for 19 out of 22 ULIRGs determined in this study are consistent with those in the literature. If we compare ULIRGs whose subclasses (see columns 11 and 12 in Table 1) were determined, 9 out of 13 ULIRGs show a good agreement. Although there are three ULIRGs with different types (or four ULIRGs with different subclasses), all of these ULIRGs are composite galaxies either in this study or in the previous studies.

4.2 Dependence of optical properties on infrared parameters

In our sample, 50% (57/115) of the ULIRGs are found to host AGN. The AGN fraction depends on the infrared luminosity and the *IRAS* flux density ratios (hereafter

IRAS colours) as follows: 48% for ULIRGs with $12.0 \leq \log(L_{\text{IR}}/L_{\odot}) < 12.15$, 50% for $[12.15, 12.4)$, and 57% for $[12.4, 13.0)$. 40% for ULIRGs with $-1.4 \leq \log(f_{25}/f_{60}) < -0.9$, 47% for $[-0.9, -0.5)$, and 92% for $[-0.5, -0.1)$. 36% for ULIRGs with $-0.7 \leq \log(f_{60}/f_{100}) < -0.3$, 33% for $[-0.3, -0.1)$, and 52% for $[-0.1, 0.3)$. The ULIRGs with a flux upper limit at 25 (100) μm are not included in the calculations for *IRAS* 25–60 (60–100) μm colour dependence. These results are summarized in Table 4 together with those from the 1 Jy (Kim & Sanders 1998) and SDSS (Hou et al. 2009) samples. Note that no ULIRGs in the 1 Jy sample have colours of $\log(f_{60}/f_{100}) < -0.3$ due to the selection criteria in Kim & Sanders (1998). The AGN fractions for each sample are comparable in the sense that the differences are less than 1.6σ by assuming Poisson errors. In all samples, there is a tendency for the ULIRGs with higher infrared luminosity, warmer *IRAS* 25–60 μm colour to be more AGN-like. These findings are consistent with those in previous works (e.g., Veilleux et al. 1999; Kewley et al. 2001; Goto 2005; Cao et al. 2006; Hou et al. 2009; Yuan et al. 2010).

In Fig. 5, we present infrared luminosity, *IRAS* 25–60 μm colour, and *IRAS* 60–100 μm colour distributions of the combined sample (432 ULIRGs) including this study, Kim & Sanders (1998), and Hou et al. (2009). Based on the Kolmogorov-Smirnov (K-S) test, we find that the infrared luminosity distribution of broad-line AGN ULIRGs is significantly different from those of non-AGN and narrow-line AGN ULIRGs, while those of non-AGN and narrow-line AGN ULIRGs are not so different. We also find that the three types of ULIRGs are significantly different from each other in *IRAS* 25–60 μm colour distribution but they are indistinguishable in *IRAS* 60–100 μm colour distribution. In *IRAS* 25–60 μm colour distribution, the significant difference between AGN and non-AGN ULIRGs strengthens that mid-infrared colour is a good indicator of AGN activity in infrared galaxies (e.g., de Grijs et al. 1985; Neff & Hutchings 1992). The little differences in *IRAS* 60–100 μm colour distribution reinforce that star formation dominates the emission of AGN in the far-infrared regime (e.g.,

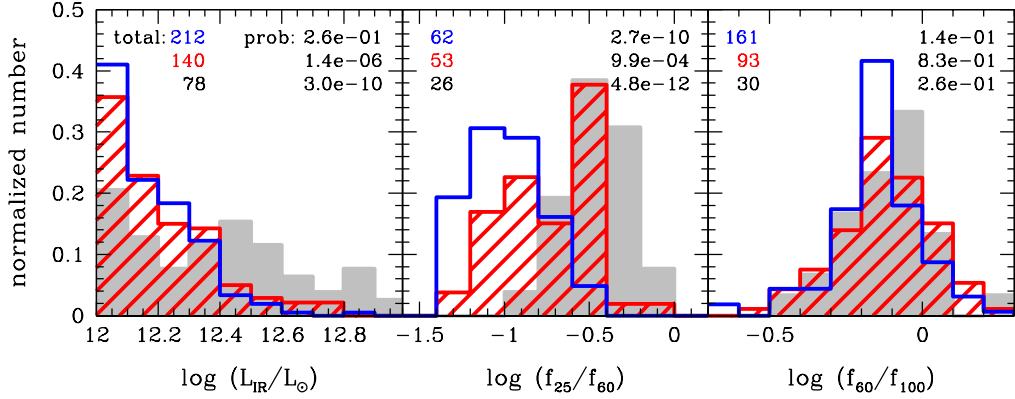


Figure 5. Infrared luminosity (left), *IRAS* 25–60 μm colour (middle), and *IRAS* 60–100 μm colour (right) distributions of the combined ULIRG sample. The distributions of non-AGN, narrow-line AGN, and broad-line AGN ULIRGs are demonstrated by solid, hatched, and shaded histograms, respectively. The ULIRGs with a flux upper limit at 25 (100) μm are not included in the middle (right) panel. The histograms are normalized to the total numbers of each spectral type, which are represented in the upper-left corner (upper: non-AGN; middle: narrow-line AGN; lower: broad-line AGN). The values in the upper-right corner show the probability that the two types of ULIRGs are drawn from the same population, given by the K-S test (Small values mean that the distributions of two types are significantly different.). The upper, middle, and lower values are calculated between non-AGNs and narrow-line AGNs, narrow-line AGNs and broad-line AGNs, and broad-line AGNs and non-AGNs, respectively.

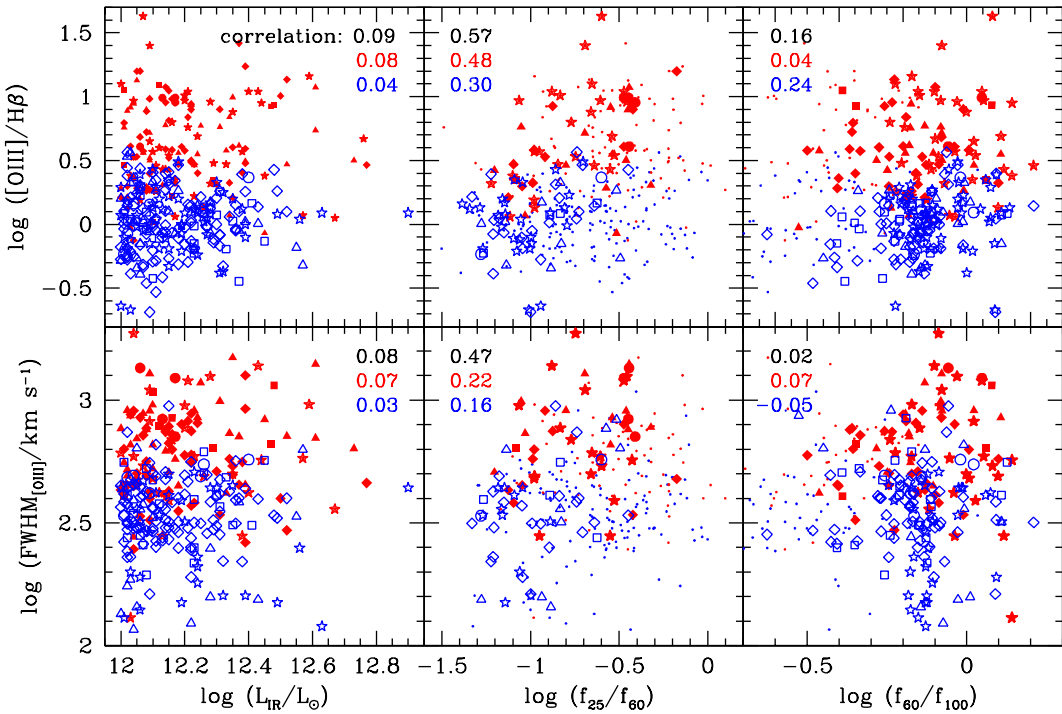


Figure 6. Relations between optical and infrared properties of narrow emission-line objects in the combined ULIRG sample. $[\text{O III}]/\text{H}\beta$ line ratio vs. infrared luminosity (upper-left), $[\text{O III}]/\text{H}\beta$ line ratio vs. the *IRAS* 25–60 μm colour (upper-middle), $[\text{O III}]/\text{H}\beta$ line ratio vs. the *IRAS* 60–100 μm colour (upper-right), $\text{FWHM}_{[\text{O III}]}$ vs. infrared luminosity (lower-left), $\text{FWHM}_{[\text{O III}]}$ vs. the *IRAS* 25–60 μm colour (lower-middle) and $\text{FWHM}_{[\text{O III}]}$ vs. the *IRAS* 60–100 μm colour (lower-right) diagrams are presented. The symbol shapes are the same as in Fig. 3. The filled and open symbols are narrow-line AGNs and non-AGNs, respectively. The values in each panel indicate Spearman’s rank correlation coefficient between two properties. The upper, middle, and lower values are calculated from narrow-line AGN plus non-AGN, narrow-line AGN, and non-AGN ULIRGs, respectively. In the middle (right) panels, the ULIRGs which have a flux upper limit at 25 (100) μm are not used in the calculations and they are represented by dots.

Elbaz et al. 2010; Hatziminaoglou et al. 2010; Hwang et al. 2010b; Shao et al. 2010). On the other hand, narrow-line AGN ULIRGs have in general lower infrared luminosity and cooler $IRAS$ 25–60 μm colour than broad-line AGN ULIRGs do. If we assume that the infrared emission in galaxies is emitted isotropically, and does not depend on viewing angle (e.g., Mulchaey et al. 1994; Schartmann et al. 2008; Gandhi et al. 2009), the difference between narrow-line AGN and broad-line AGN ULIRGs seems not to be compatible with the predictions of the orientation-dependent unification model of AGNs in which narrow-line and broad-line AGNs are intrinsically same objects observed from different angles (Antonucci 1993). This conflict can be explained if narrow-line AGN ULIRGs host a central engine deeply buried by extended, dusty regions of star formation as proposed by several authors (e.g., Genzel et al. 1998; Gerssen et al. 2004).

In Fig. 6, we show the relations between optical ($[\text{O III}]/\text{H}\beta$ line ratio or $[\text{O III}]$ line width) and infrared (infrared luminosity, $IRAS$ 25–60 μm colour or $IRAS$ 60–100 μm colour) properties of the combined ULIRG sample. Broad-line AGN ULIRGs are not plotted because their line widths and fluxes are not properly measured in many cases³. Since the spectral types are determined by the optical emission lines, narrow-line AGNs and non-AGNs are well separated along the y-axis. As expected, clear correlations are found only in the middle panels (see the values of Spearman's rank correlation coefficients). We checked these relations using various infrared colours from the *AKARI* all-sky survey point source catalogues⁴ but we could not draw any meaningful results due to the small number of data points.

5 SUMMARY

We studied optical spectral properties of 115 southern ULIRGs using the spectra obtained from our CTIO observations, 2dFGRS, and 6dFGS. For ULIRGs with $\text{H}\alpha$ measurement, we classified them in the standard diagnostic diagrams. We classified the other ULIRGs using the $[\text{O III}]\lambda 5007/\text{H}\beta$ line ratio against $[\text{O III}]\lambda 5007$ line width diagram with an empirically determined criterion. Main results are summarized below.

(i) Our new criterion, $\log ([\text{O III}]/\text{H}\beta) > -0.13$ ($\text{FWHM}_{[\text{O III}]} / 100 \text{ km s}^{-1} + 0.85$), is successful to separate AGN ULIRGs from non-AGN ULIRGs with completeness and reliability of about 90%.

(ii) In our sample of the 115 ULIRGs, there are 8 broad-line AGNs, 49 narrow-line AGNs, and 58 non-AGNs. The AGN fraction is 50% and changes as a function of infrared luminosity and $IRAS$ 25–60 μm colour. These results are consistent with those in previous studies.

(iii) Using the combined ULIRG sample, we show that the colour distributions of AGN and non-AGN ULIRGs are significantly different in $IRAS$ 25–60 μm colour and are indistinguishable in $IRAS$ 60–100 μm colour. These results

³ The spectra of broad-line AGNs should be analysed with more sophisticated methods of galaxy modelling (e.g., Kim et al. 2006).

⁴ <http://www.ir.isas.jaxa.jp/AKARI/Observation/PSC/Public/>

support that mid-infrared colour is sensitive to AGN activity, whereas far-infrared colour is dominated by star formation.

(iv) We also show that broad-line AGN ULIRGs differ from narrow-line AGN ULIRGs in infrared luminosity and $IRAS$ 25–60 μm colour. This presents a challenge to the simple unification model of AGNs.

ACKNOWLEDGMENTS

We thank the CTIO staff for their help on the observations. We also thank L. G. Hou for providing the $[\text{O III}]$ line width data of the SDSS ULIRGs. We are grateful to anonymous referee whose comments helped to improve the original manuscript. This work was supported by Mid-career Research Program through NRF grant funded by the MEST (No.2010-0013875). H.S.H acknowledges the support of the Centre National d'Etudes Spatiales (CNES). S.C.K is a member of the Dedicated Researchers for Extragalactic AstronoMy (DREAM) team in Korea Astronomy and Space Science Institute (KASI).

REFERENCES

- Adelman-McCarthy J. K. et al., 2006, ApJS, 162, 38
- Allen D. A., Norris R. P., Meadows V. S., Roche P. F., 1991, MNRAS, 248, 528
- Antonucci R., 1993, ARA&A, 31, 473
- Baldwin J. A., Phillips M. M., Terlevich R., 1981, PASP, 93, 5
- Barnes J. E., 2004, MNRAS, 350, 798
- Brinchmann J., Kunth D., Durret F., 2008, A&A, 485, 657
- Bushouse H. A., 1987, ApJ, 320, 49
- Cao C., Wu H., Wang J. L., Hao C. N., Deng Z. G., Xia X. Y., Zou Z. L., 2006, ChJAA, 6, 197
- Cardelli J. A., Clayton G. C., Mathis J. S., 1989, ApJ, 345, 245
- Clements D. L., Sutherland W. J., McMahon R. G., Saunders W., 1996, MNRAS, 279, 477
- Colless M. et al., 2001, MNRAS, 328, 1039
- Dasyra K. M. et al., 2006, ApJ, 638, 745
- de Grijp M. H. K., Miley G. K., Lub J., de Jong T., 1985, Nature, 314, 240
- Duc P.-A., Mirabel I. F., Maza J., 1997, A&AS, 124, 533
- Elbaz D. et al., 2010, A&A, 518, L29
- Farrah D. et al., 2007, ApJ, 667, 149
- Franceschini A. et al., 2003, MNRAS, 343, 1181
- Gandhi P. et al., 2009, A&A, 502, 457
- Genzel R. et al., 1998, ApJ, 498, 579
- Genzel R., Tacconi L. J., Rigopoulou D., Lutz D., Tecza M., 2001, ApJ, 563, 527
- Gerssen J., van der Marel R. P., Axon D., Mihos J. C., Hernquist L., Barnes J. E., 2004, AJ, 127, 75
- Goto T., 2005, MNRAS, 360, 322
- Greene J. E., Ho L. C., 2005, ApJ, 627, 721
- Hao L. et al., 2005, AJ, 129, 1783
- Hatziminaoglou E. et al., 2010, A&A, 518, L33
- Heckman T. M., Miley G. K., van Breugel W. J. M., Butcher H. R., 1981, ApJ, 247, 403
- Hopkins A. M. et al., 2003, ApJ, 599, 971

- Hopkins P. F., Somerville R. S., Hernquist L., Cox T. J., Robertson B., Li Y., 2006, ApJ, 652, 864
- Hou L. G., Wu X., Han J. L., 2009, ApJ, 704, 789
- Hwang H. S., Elbaz D., Lee J. C., Jeong W.-S., Park C., Lee M. G., Lee H. M., 2010a, A&A, 522, A33
- Hwang H. S. et al., 2010b, MNRAS, 409, 75
- Hwang H. S., Serjeant S., Lee M. G., Lee K. H., White G. J., 2007, MNRAS, 375, 115
- Imanishi M., Maiolino R., Nakagawa T., 2010, ApJ, 709, 801
- Jones D. H., Saunders W., Read M., Colless M., 2005, PASA, 22, 277
- Jones D. H. et al. 2004, MNRAS, 355, 747
- Kauffmann G. et al., 2003, MNRAS, 346, 1055
- Kewley L. J., Groves B., Kauffmann G., Heckman T., 2006, MNRAS, 372, 961
- Kewley L. J., Heisler C. A., Dopita M. A., Lumsden S., 2001, ApJS, 132, 37
- Kewley L. J., Jansen R. A., Geller M. J., 2005, PASP, 117, 227
- Kim D.-C., Sanders D. B., 1998, ApJS, 119, 41
- Kim D.-C., Veilleux S., Sanders D. B., 1998, ApJ, 508, 627
- Kim M., Ho L. C., Im M., 2006, ApJ, 642, 702
- Le Floc'h E. et al., 2005, ApJ, 632, 169
- Liu C. T., Kennicutt R. C., 1995, ApJS, 100, 325
- Lonsdale C. J., Farrah D., Smith H. E., 2006, in Mason J. W., ed., *Astrophysics Update 2: Topical and Timely Reviews on Astronomy and astrophysics*. Springer, Berlin, p.285
- Low F. J., Cutri R. M., Huchra J. P., Kleinmann S. G., 1988, ApJL, 327, 41
- Magnelli B., Elbaz D., Chary R. R., Dickinson M., Le Borgne D., Frayer D. T., Willmer C. N. A., 2009, A&A, 496, 57
- Markwardt C. B., 2009, in Bohlender D. A., Durand D., Dowler P., eds, ASP conf. Ser. Vol. 411, Astron. Soc. Pac., San Francisco, p. 251
- Massey P., Strobel K., Barnes J. V., Anderson E., 1988, ApJ, 328, 315
- Mihos J. C., Hernquist L., 1996, ApJ, 464, 641
- Miller N. A., Owen F. N., 2002, AJ, 124, 2453
- Moshir M. et al., 1992, Explanatory Supplement to the *IRAS* Faint Source Survey, Version 2, JPL D-10015 8/92. JPL, Pasadena
- Mouhcine M., Lewis I., Jones B., Lamareille F., Maddox S. J., Contini T., 2005, MNRAS, 362, 1143
- Mulchaey J. S. et al., 1994, ApJ, 436, 586
- Nagar N. M., Wilson A. S., Falcke H., Veilleux S., Maiolino R., 2003, A&A, 409, 115
- Neff S. G., Hutchings J. B., 1992, AJ, 103, 1746
- Neugebauer G. et al., 1984, ApJ, 278, L1
- Osterbrock D. E., Cohen R. D., 1982, ApJ, 261, 64
- Osterbrock D. E., Ferland G. J., 2006, *Astrophysics of Gaseous Nebulae and Active Galactic Nuclei*, 2nd edn. University Science Books, Mill Valley, CA
- Osterbrock D. E., Mathews W. G., 1986, ARA&A, 24, 171
- Owers M. S., Blake C., Couch W. J., Pracy M. B., Bekki K., 2007, MNRAS, 381, 494
- Pasquali A., Kauffmann G., Heckman T. M., 2005, MNRAS, 361, 1121
- Risaliti G. et al., 2006, MNRAS, 365, 303
- Sajina A. et al. 2008, ApJ, 683, 659
- Sanders D. B., Mazzarella J. M., Kim D.-C., Surace J. A., 2003, AJ, 126, 1607
- Sanders D. B., Mirabel I.F., 1996, ARA&A, 34, 749
- Sanders D. B., Soifer B. T., Elias J. H., Madore B. F., Matthews K., Neugebauer G., Scoville N. Z., 1988, ApJ, 325, 74
- Schartmann M., Meisenheimer K., Camenzind M., Wolf S., Tristram K. R. W., Henning T., 2008, A&A, 482, 67
- Schlegel D. J., Finkbeiner D. P., Davis M., 1998, ApJ, 500, 525
- Shao L. et al., 2010, A&A, 518, L26
- Soifer B. T., Sanders D. B., Madore B. F., Neugebauer G., Danielson G. E., Elias J. H., Lonsdale C. J., Rice W. L., 1987, ApJ, 320, 238
- Tacconi L. J., Genzel R., Lutz D., Rigopoulou D., Baker A. J., Iserlohe C., Tecza M., 2002, ApJ, 580, 73
- Teng S. H. et al., 2009, ApJ, 691, 261
- Veilleux S., Kim D.-C., Sanders D. B., 1999, ApJ, 522, 113
- Veilleux S., Kim D.-C., Sanders D. B., 2002, ApJS, 143, 315
- Veilleux S., Osterbrock D. E., 1987, ApJS, 63, 295
- York D. G. et al., 2000, AJ, 120, 1579
- Younger J. D., Hayward C. C., Narayanan D., Cox T. J., Hernquist L., Jonsson P., 2009, MNRAS, 396, 66
- Yuan T.-T., Kewley L. J., Sanders D. B., 2010, ApJ, 709, 884
- Zakamska N. L. et al., 2003, AJ, 126, 2125